Perturbing the Hydrophobic Pocket of Mandelate Racemase To Probe Phenyl Motion during Catalysis†

Ferhan Siddiqi,‡ Jennifer R. Bourque,‡ Haiyan Jiang,§ Marieke Gardner,‡ Martin St. Maurice,‡ Christian Blouin,‡,§ and Stephen L. Bearne*,‡

Department of Biochemistry and Molecular Biology and Faculty of Computer Science, Dalhousie University, Halifax, Nova Scotia B3H 1X5, Canada

Received December 21, 2004; Revised Manuscript Received May 4, 2005

ABSTRACT: Mandelate racemase (MR, EC 5.1.2.2) from *Pseudomonas putida* catalyzes the Mg^{2+}-dependent 1,1-proton transfer that interconverts the enantiomers of mandelate. Crystal structures of MR reveal that the phenyl group of all ground-state ligands is located within a hydrophobic cavity, remote from the site of proton abstraction. MR forms numerous electrostatic and H-bonding interactions with the α-OH and carboxyl groups of the substrate, suggesting that these polar groups may remain relatively fixed in position during catalysis while the phenyl group is free to move between two binding sites [i.e., the *R*-pocket and the *S*-pocket for binding the phenyl group of (*R*)-mandelate and (*S*)-mandelate, respectively]. We show that MR binds benzilate ($K_i = 0.67 \pm 0.12$ mM) and (*S*)-cyclohexylphenylglycolate ($K_i = 0.50 \pm 0.03$ mM) as competitive inhibitors with affinities similar to that which the enzyme exhibits for the substrate. Therefore, the active site can simultaneously accommodate two phenyl groups, consistent with the existence of an *R*-pocket and an *S*-pocket. Wild-type MR exhibits a slightly higher affinity for (*S*)-mandelate [i.e., $K_m^{(S)-man} < K_m^{(R)-man}$] but catalyzes the turnover of (*R*)-mandelate slightly more rapidly (i.e., $k_{cat}^{R\rightarrow S} > k_{cat}^{S\rightarrow R}$). Upon introduction of steric bulk into the *S*-pocket using site-directed mutagenesis (i.e., the F52W, Y54W, and F52W/Y54W mutants), this catalytic preference is reversed. Although the catalytic efficiency (k_{cat}/K_m) of all the mutants was reduced (11−280-fold), all mutants exhibited a higher affinity for (*R*)-mandelate than for (*S*)-mandelate, and higher turnover numbers with (*S*)-mandelate as the substrate, relative to those with (*R*)-mandelate. (*R*)- and (*S*)-2-hydroxybutyrate are expected to be less sensitive to the additional steric bulk in the *S*-pocket. Unlike those for mandelate, the relative binding affinities for these substrate analogues are not reversed. These results are consistent with steric obstruction in the *S*-pocket and support the hypothesis that the phenyl group of the substrate may move between an *R*-pocket and an *S*-pocket during racemization. These conclusions were also supported by modeling of the binary complexes of the wild-type and F52W/Y54W enzymes with the substrate analogues (*R*)- and (*S*)-atrolactate, and of wild-type MR with bound benzilate using molecular dynamics simulations.

Mandelate racemase (MR,[1] EC 5.1.2.2) from *Pseudomonas putida* catalyzes the Mg^{2+}-dependent 1,1-proton transfer that interconverts the enantiomers of mandelate (Scheme 1) (*1*). Isotope exchange experiments, site-directed mutagenesis, and X-ray crystal structures of MR complexed with the substrate and substrate analogues (*2*−*6*) indicate that catalysis proceeds via a two-base mechanism, with His 297 and Lys 166 abstracting the α-proton from (*R*)-mandelate and (*S*)-mandelate, respectively (*3*, *4*, *7*). In addition, these experiments

Scheme 1

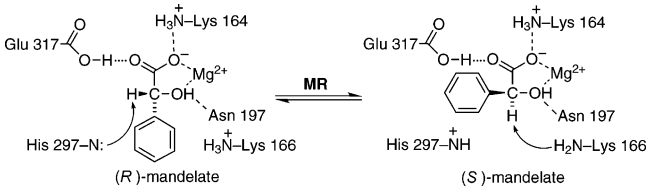

have revealed that Glu 317 acts as an electrophilic catalyst (*5*), Lys 164 interacts with the carboxyl function of mandelate (*2*), and Asn 197 interacts with the α-hydroxyl of mandelate to facilitate stabilization of the altered substrate in the transition state (*8*). The ability of MR to catalyze rapid carbon−hydrogen bond cleavage from a carbon acid with a relatively high pK_a (*9*−*11*) makes it a useful paradigm for understanding enzyme-catalyzed proton abstraction from carbon acids (*1*, *10*, *12*−*14*).

MR is extremely proficient at discriminating between the substrate in the ground state and the altered substrate in the transition state, binding the latter with an apparent association constant equal to 5×10^{18} M^{-1} and stabilizing the transition

† This work was supported by Discovery Grants (S.L.B. and C.B.) from the Natural Sciences and Engineering Research Council (NSERC) of Canada. M.St.M. was the recipient of an NSERC postgraduate scholarship, and F.S. and M.G. were recipients of NSERC undergraduate summer research awards. H.J. was supported by a grant from Genome Atlantic (to C.B.).

* To whom correspondence should be addressed. Phone: (902) 494-1974. Fax: (902) 494-1355. E-mail: sbearne@dal.ca.

‡ Department of Biochemistry and Molecular Biology.

§ Faculty of Computer Science.

[1] Abbreviations: BSA, bovine serum albumin; (*S*)-CHPG, (*S*)-cyclohexylphenylglycolate; CD, circular dichroism; HEPES, 4-(2-hydroxyethyl)piperazine-1-ethanesulfonic acid; MD, molecular dynamics; MR, mandelate racemase.

10.1021/bi0473096 CCC: $30.25
Published on Web 06/03/2005

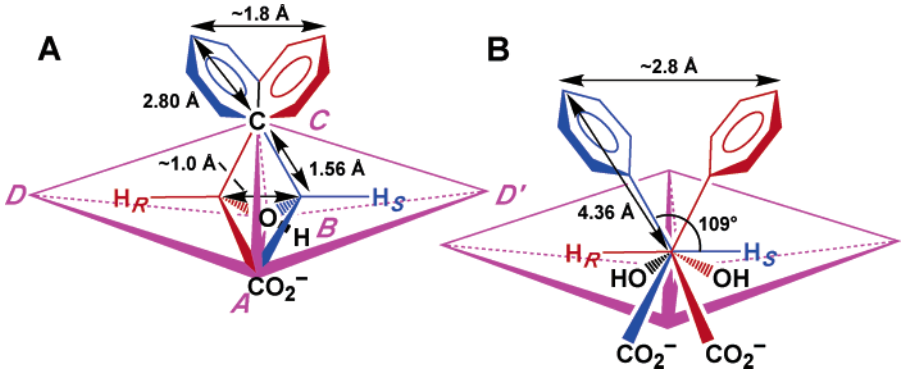

FIGURE 1: Motion of the phenyl group during catalysis. (*R*)- and (*S*)-mandelate are shown bound at the active site of MR using the four-location model of Mesecar and Koshland (*41*). The carboxylate, hydroxyl, and phenyl groups are bound within the same plane (sites *A*−*C*), while the α-proton may interact with either of two sites (*D* or *D*′) depending on the enantiomer that is bound. Bond lengths derived from the crystal structure of MR with bound (*S*)-atrolactate may be used to estimate the distance that the para carbon atom of the phenyl ring moves during catalysis. If the carboxylate, hydroxyl, and *β*-carbon of (*R*)- and (*S*)-mandelate are bound within the same plane (A) and the α-carbon moves (∼1.0 Å) as it undergoes a Walden inversion, then the para carbon atom of the phenyl ring may move ∼1.8 Å during catalysis. On the other hand, if the carboxylate, hydroxyl, and *β*-carbon groups move slightly to either side of the plane and the position of the α-carbon remains fixed (B), then the para carbon atom of the phenyl ring may move ∼2.8 Å during catalysis.

state for the reaction by 26 kcal/mol (*15*). The high proficiency of MR is achieved principally by enthalpy reduction, with enthalpy providing nearly 23 kcal/mol to the apparent binding free energy of the altered substrate in the transition state (*16*). This substantial release of energy is compatible with the development of enhanced hydrogen bonding, electrostatic interactions, and nonpolar interactions in the enzyme−transition-state complex (*17*). The numerous electrostatic interactions between the ligand and polar residues within the active site that contribute to ground-state binding and transition-state stabilization are shown in Scheme 1. These multiple electrostatic interactions might be expected to hold the carboxylate and α-hydroxyl functions of the substrate anchored in place as shown in Figure 1A. The α-carbon may then undergo motion as the substrate enantiomer is converted into the product enantiomer. If the *β*-carbon (carbon 1 of the phenyl ring) remains stationary but pivots with the motion of the α-carbon, then the para carbon of the phenyl ring might only traverse ∼1.8 Å during catalysis. However, if the α-carbon remains fixed in position while the *β*-carbon, hydroxyl group, and carboxylate group move, then the para carbon of the phenyl ring might traverse ∼2.8 Å during catalysis (Figure 1B).

To date, all crystal structures of MR complexes have either (*S*)-mandelate or analogues of (*S*)-mandelate bound at the active site. In addition to the polar region that binds the α-hydroxyl and carboxylate functions of mandelate, these structures reveal the presence of a hydrophobic pocket that binds the phenyl group. The observation that MR can utilize a variety of aryl- and heteroaryl-substituted mandelate derivatives as substrates supports the notion that this hydrophobic pocket is quite plastic and could accommodate the motion of the phenyl ring (*18*, *19*). We propose that the phenyl group may move between two binding sites within the hydrophobic pocket during catalysis. Initially, the phenyl group of either (*R*)- or (*S*)-mandelate is bound at its corresponding site (i.e., the *R*- or *S*-pocket, respectively). The phenyl group then moves through the hydrophobic pocket to form a planar intermediate upon substrate deprotonation, and then comes to rest in the pocket for the product enantiomer after stereospecific reprotonation.

Herein, we present evidence supporting our hypothesis that the phenyl ring moves within the active site of MR during catalysis. First, we report that MR binds the substrate-product analogues benzilate and (*S*)-cyclohexylphenylglycolate [(*S*)-CHPG] with affinities that equal or slightly exceed that which the enzyme exhibits for the substrate. These findings support the notion that the hydrophobic pocket within the active site of MR can simultaneously accommodate two phenyl groups, consistent with the existence of an *R*-pocket and an *S*-pocket. Second, we use site-directed mutagenesis to introduce steric hindrance within the *S*-pocket (i.e., the F52W, Y54W, and F52W/Y54W mutants). The mutants exhibited a higher affinity for (*R*)-mandelate than for (*S*)-mandelate, and higher turnover numbers with (*S*)-mandelate as the substrate, relative to that with (*R*)-mandelate. We also show that, unlike mandelate, the substrate analogues (*R*)- and (*S*)-2-hydroxybutyrate, which are expected to be less sensitive to the additional steric bulk in the *S*-pocket, do not exhibit reversal of their relative binding affinities. These results are consistent with steric obstruction in the *S*-pocket and movement of the phenyl group between an *R*-pocket and an *S*-pocket during racemization. Finally, we use molecular dynamics simulations to model the binary complexes of wild-type and F52W/Y54W enzymes with the substrate analogues (*R*)- and (*S*)-atrolactate.

MATERIALS AND METHODS

(*R*)- and (*S*)-2-naphthylglycolic acid were prepared as described previously (*19*). (*S*)-CHPG was a generous gift from Sepracor Canada Ltd. (Windsor, NS). All other reagents, unless mentioned otherwise, were purchased from Sigma-Aldrich Canada Ltd. (Oakville, ON). Deoxyoligonucleotide primers were commercially synthesized by ID Laboratories (London, ON). The QIAprep spin plasmid miniprep kit (Qiagen Inc., Mississauga, ON) was used for the preparation of plasmids for mutagenesis and transformation. Recombinant MR from *P. putida* was overexpressed in and purified from *Escherichia coli* strain BL21(DE3) cells transformed with a pET15b plasmid (Novagen, Madison, WI) containing the MR open reading frame (ORF) (*8*). This construct encodes the MR gene product with an N-terminal hexahistidine tag [MGSS$(H)_6$SSGLVPRGSHM$_1$...MR]. The

enzyme was purified by metal ion affinity chromatography as described previously (*8*). The presence or absence of the hexahistidine tag does not influence the kinetic parameters for the recombinant enzyme (*20*). Circular dichroism (CD) assays and spectral measurements were conducted using a JASCO J-810 spectropolarimeter.

Site-Directed Mutagenesis. The pET-15b plasmid bearing the recombinant MR open reading frame was used as the template for polymerase chain reaction-based site-directed mutagenesis using the QuickChange Site-Directed Mutagenesis Kit (Stratagene, La Jolla, CA) following the protocols described by the manufacturer. The forward (F) and reverse (R) synthetic deoxyoligonucleotide primers used to construct the mutants were as follows: 5′-dCCATTCCTACCTGTGGGCATACACCCCCG-3′ (F, F52W), 5′-dCGGGGGTGTATGCCCACAGGTAGGAATGG-3′ (R, F52W), 5′-dCATTCCTACCTGTTCGCATGGACCCCCGTTGCGTTG-3′ (F, Y54W), 5′-dCAACGCAACGGGGGTCCATGCGAACAGGTAGGAATG-3′ (R, Y54W), 5′-dCATTCCTACCTGTGGGCATGGACCCCCGTTGCGTTGAAG-3′ (F, F52W/Y54W), and 5′-dCTTCAACGCAACGGGGGTCCATGCCCACAGGTAGGAATG-3′ (R, F52W/Y54W). The mismatched bases are underlined. Potential mutant plasmids were isolated and used to transform competent DH5α cells. These cells were used for plasmid maintenance and for all sequencing reactions. Each mutant ORF was sequenced using commercial automated sequencing (Robarts Research Institute, London, ON) to ensure that no other alterations of the nucleotide sequence had been introduced. Competent *E. coli* strain BL21(DE3) cells were used as the host for target gene expression.

Enzyme Assays. MR activity was assayed using the circular dichroism (CD) assay by following the change in ellipticity at 262 nm as described by Sharp et al. (*21*). All inhibition assays were conducted at 25 °C in Na^+-HEPES buffer (0.1 M, pH 7.5) containing $MgCl_2$ (3.3 mM, unless mentioned otherwise) and bovine serum albumin (BSA, 0.005%). The concentrations of (*R*)- and (*S*)-mandelate for assays of wild-type MR and F52W were 0.19, 0.38, 0.57, 0.76, 0.95, 2.38, 4.75, 7.13, and 9.5 mM. Y54W was assayed using concentrations for (*R*)- and (*S*)-mandelate equal to 0.24, 0.48, 0.95, 2.375, 4.75, 7.13, 9.5, and 15 ($S \rightarrow R$ only) mM with the concentration of $MgCl_2$ equal to 15 mM. Substrate concentrations for assays of F52W/Y54W activity were 0.095, 0.19, 0.285, 0.475, 0.95, 2.375, 4.75, 7.125, and 9.5 mM for (*R*)-mandelate and 0.238, 0.475, 0.95, 2.375, 4.75, 7.125, 9.5, 14.25, and 19 mM for (*S*)-mandelate. Substrate solutions were incubated at 25 °C for 5 min prior to initiation of the reaction by addition of enzyme. The final concentrations of wild-type MR and F52W were 0.15 and 0.30 μg/mL. The final concentrations of enzyme were 10 and 15 μg/mL for Y54W and 21.2 and 10.5 μg/mL for F52W/Y54W, in the $R \rightarrow S$ and $S \rightarrow R$ directions, respectively.

For assays with the substrates (*R*)- and (*S*)-2-naphthylglycolic acid, the reactions were followed at 266 nm in a quartz cuvette with a 0.1 cm light path as described previously (*19*). The substrate concentrations were 0.10, 0.25, 0.50, 1.0, 2.5, 5.0, and 7.5 mM, and the concentration of F52W/Y54W was 22.3 μg/mL.

Inhibition Assays. MR activity for both wild-type MR and F52W was assayed in the $R \rightarrow S$ direction using concentrations of (*R*)-mandelate equal to 0.238, 0.475, 0.95, 2.38, and 4.75 mM. Concentrations of benzohydroxamate were 0, 5, 10, and 20 μM for assays of wild-type MR and 0, 5, 10, 15, 20, and 30 μM for assays of F52W. Reactions were initiated by addition of enzyme, giving final concentrations of 0.1 and 0.9 μg/mL for wild-type MR and F52W, respectively.

Inhibition assays using the F52W/Y54W mutant enzyme were conducted using (*S*)-mandelate as the substrate because the turnover number of this enzyme with (*S*)-mandelate was greater than that observed with (*R*)-mandelate. Concentrations of (*S*)-mandelate were 0.5, 1.0, 2.5, 5.0, 7.5, 10, and 15 mM for assays of F52W/Y54W activity. For assays with Y54W, the concentrations of (*R*)-mandelate were 0, 0.25, 0.50, 1.0, 2.5, 5.0, and 7.5 mM with the concentration of $MgCl_2$ equal to 15 mM. Concentrations of benzohydroxamate were 0, 0.05, 0.10, and 0.20 mM for assays of Y54W MR activity and 0, 0.25, 0.50, and 1.00 mM for assays of F52W/Y54W activity. Reactions were initiated by addition of either Y54W or F52W/Y54W to give a final enzyme concentration of 5 or 10 μg/mL, respectively.

The inhibition of wild-type MR by benzilate, (*S*)-CHPG, and diphenylacetate was examined using (*R*)-mandelate as the substrate, unless mentioned otherwise. For benzilate, the CD assay was conducted at 268 nm ($[\theta]^R_{268} = 2980$ deg mol^{-1} cm^2) because of the high absorbance at 262 nm. The concentrations of benzilate used in inhibition assays with the wild-type enzyme were 0, 0.48, 0.95, and 1.90 mM. For the inhibition of F52W/Y54W by benzilate, only a single concentration of benzilate (10.0 mM) was used to estimate the value of the competitive inhibition constant with respect to (*S*)-mandelate (0.5, 1.0, 2.0, 5.0, and 10.0 mM) because of the high absorbance exhibited by benzilate at 268 nm. The concentrations of (*S*)-CHPG used in inhibition assays were 0, 0.24, 0.48, and 0.71 mM. Inhibition assays with diphenylacetate contained DMSO (15%) and were conducted using a single concentration of diphenylacetate (2.0 mM) because of the high absorbance of this compound. The K_i value for diphenylacetate was estimated from the change in observed initial velocities assuming competitive inhibition. The inhibition of wild-type MR by (*R*)-2-hydroxybutyrate (0, 5, 10, and 15 mM) and (*S*)-2-hydroxybutyrate (0, 5, 10, and 15 mM) was assayed using (*R*)-mandelate (0.5, 1.0, 2.0, 5.0, and 10.0 mM) with a final enzyme concentration of 0.15 μg/mL. The inhibition of F52W/Y54W by (*R*)-2-hydroxybutyrate (0, 60, and 90 mM) and (*S*)-2-hydroxybutyrate (0, 20, 40, and 60 mM) was assayed using (*S*)-mandelate (0.5, 1.0, 2.0, 5.0, and 10.0 mM) with a final enzyme concentration of 8.8 μg/mL.

Data Analysis and Protein Concentrations. The values of V_{max} and K_m were determined from plots of the initial velocity (v_i) versus substrate concentration ([S]) by fitting the data to eq 1 using nonlinear regression analysis and *KaleidaGraph* version 3.5 from Synergy Software (Reading, PA). Competitive inhibition constants (K_i) were determined from linear replots of the observed values of K_m/V_{max} versus inhibitor concentration ([I]) according to eq 2. All kinetic parameters were determined in triplicate, and average values are reported. The reported errors are standard deviations. Protein concentrations were determined using the Bio-Rad protein assay (Bio-Rad Laboratories, Mississauga, ON) with BSA standards, and k_{cat} values were obtained by dividing V_{max} values by the total enzyme concentration ($[E]_t$) using molecular masses of 40 728, 40 767, 40 751, and 40 790 Da

for wild-type, F52W, Y54W, and F52W/Y54W mandelate racemases, respectively.

$$v_i = \frac{V_{max}[S]}{K_m + [S]} \quad (1)$$

$$v_i = \frac{V_{max}[S]}{K_m\left(1 + \frac{[I]}{K_i}\right) + [S]} \quad (2)$$

Magnesium Ion Binding. The apparent K_m value for Mg^{2+} was determined for both wild-type and mutant enzymes using the method described by Fee et al. (*22*). Enzyme, freed of Mg^{2+} by exhaustive dialysis against Na^+-HEPES buffer (0.1 M, pH 8.0) containing EDTA (5 mM) followed by dialysis against Na^+-HEPES buffer (0.1 M, pH 7.5), was first incubated with the desired concentration of $MgCl_2$ for 5 min, and then the reaction was initiated by addition of either (*R*)- or (*S*)-mandelate (final concentration of 10 mM). For wild-type MR (150 ng/mL) and F52W (1.6 μg/mL), the concentrations of $MgCl_2$ that were used were 0.05, 0.10, 0.15, 0.25, 0.50, 1.0, and 2.5 mM and the substrate was (*R*)-mandelate. For Y54W (10.75 μg/mL), the concentrations of $MgCl_2$ that were used were 0.10, 0.25, 0.50, 1.0, 2.5, 4.0, 8.0, 12.0, 15.0, and 20.0 mM and the substrate was (*R*)-mandelate. For F52W/Y54W (12.6 μg/mL), the concentrations of $MgCl_2$ that were used were 0.05, 0.10, 0.15, 0.20, 0.50, 1.0, and 2.5 mM and the substrate was (*S*)-mandelate.

Circular Dichroism. Solutions of wild-type MR (50.8 μg/mL) and the F52W (68.3 μg/mL), Y54W (79.1 μg/mL), and F52W/Y54W (73.9 μg/mL) enzymes were dialyzed against potassium phosphate buffer (25 mM, pH 7.5) containing $MgSO_4$ (10 mM). Protein concentrations were determined as described above except that BSA standards in potassium phosphate buffer (25 mM, pH 7.5) containing $MgSO_4$ (10 mM) were used. The CD spectra of each enzyme and the buffer were recorded over a wavelength range from 185 to 260 nm using a quartz cuvette with a 0.1 cm light path. CD spectra, obtained after subtraction of the ellipticity corresponding to the buffer, were analyzed for percent α-helix and β-sheet structure using *CDNN CD Spectra Deconvolution* version 2.1 developed by Böhm (*23*).

Computer Modeling. The binding of (*S*)-atrolactate and (*R*)-atrolactate to both wild-type MR and F52W/Y54W and binding of benzilic acid to wild-type MR were simulated by molecular dynamics (MD) using the CHARMM 3.0b1 software package (*24*) and the CHARMM22 force field (*25*). Protein Data Bank entry 1MDR (*4*) was used as the model of wild-type MR. The structure of the double mutant was obtained by replacing both Phe 52 and Tyr 54 of the wild-type model with tryptophan residues. All the crystal water molecules were deleted except for the water molecule bound to Mg^{2+} in the active site. Since Leu 93 from a 2-fold related subunit in the octamer forms part of the hydrophobic pocket within the active site of MR (*2*), residues 86−101 from the related subunit were added to the protein model.

The topology files of (*S*)-atrolactate and (*R*)-atrolactate were built manually according to their structure properties. Atom partial charges were generated using the Dundee PROG server (*26*). The force field parameters with the atom types most similar to those of atrolactate were selected from the CHARMM22 parameter files. Solvation energies were calculated using the generalized Born method (*27*).

A sphere with a radius of 12 Å was defined around the β-carbon atom of (*S*)-atrolactate, and only atoms within this sphere were allowed to move during the simulation. This sphere contained all the residues within the active site. An initial energy minimization was conducted using iterations of the conjugate gradient method and the adopted basis Newton−Raphson method until convergence was obtained. The MD simulation was then performed on these minimized structures. The positions of protein residues lying outside the 12 Å sphere were constrained with a harmonic force constant equal to 1000 kcal mol^{-1} $Å^{-2}$.

During the MD simulation, (*S*)-atrolactate was observed to drift approximately 0.8 Å from its location in the X-ray structure of the wild-type•(*S*)-atrolactate complex. Assuming that atrolactate coordinates the Mg^{2+}, we applied distance constraints equal to 2.27 and 2.39 Å between the active site magnesium and the α-hydroxyl oxygen atom of (*S*)-atrolactate and (*R*)-atrolactate in the MR•(*S*)-atrolactate and MR•(*R*)-atrolactate complexes, respectively (*28*). This restraint reduced the observed drift of the ligand so that the calculated structure of the wild-type•(*S*)-atrolactate complex was in agreement with the crystal structure. However, the (*S*)-atrolactate [or (*R*)-atrolactate] molecule still had freedom to move within the active site of the mutant MR complex. A minimal harmonic force constant was set to the value of 5 kcal mol^{-1} $Å^{-2}$ obtained by testing. The bonds to hydrogen were constrained using the Shake algorithm (*29*).

The system was heated from 0 to 300 K using 300 steps of 10 K each with 1 fs per step. The system was then equilibrated for 20 ps at 300 K, followed by an 80 ps MD simulation. The average structure was calculated from the trajectory file obtained in this simulation.

RESULTS AND DISCUSSION

Crystal structures of wild-type and mutant forms of MR complexed with substrate and substrate analogues (*3*−*6*) reveal the aromatic ring of all ground-state ligands located within a large hydrophobic cavity at the mouth of the enzyme active site, remote from the site of proton abstraction (*2*). The cavity is composed of hydrophobic amino acid residues from both the N-terminal and central β-barrel domains of the enzyme, and also includes Leu 93 from an adjacent 2-fold related subunit (*2*). A major component of the hydrophobic cavity is a large, mobile, amphipathic β-meander flap that extends over the active site (*2*). The hydrophobic cavity can accommodate a variety of aryl- and heteroaryl-substituted mandelate derivatives that serve as substrates (*16*, *18*, *30*−*33*). Steric constraints within the hydrophobic cavity appear to be more relaxed in the enzyme−substrate complex than those in the enzyme−intermediate complex (*19*). Since there are numerous polar interactions that appear to fix the positions of the carboxylate and α-hydroxyl groups of mandelate within the active site (Scheme 1), we propose that the phenyl group moves between two binding sites within the hydrophobic pocket during catalysis [i.e., the *R*-pocket and *S*-pocket for binding the phenyl group of (*R*)-mandelate and (*S*)-mandelate, respectively].

Substrate-Product Analogues. To test our hypothesis, we examined the interaction of MR with benzilate and (*S*)-

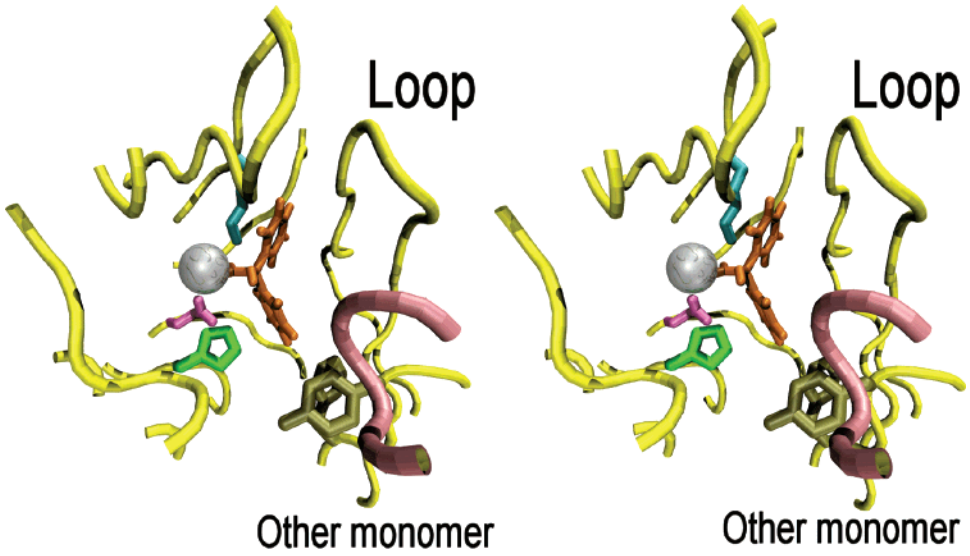

FIGURE 2: Stereoview of benzalate modeled into the active site of mandelate racemase. The polypeptide backbone of the protein is colored yellow, and catalytic residues His 297, Lys 166, and Glu 317 are colored green, blue, and magenta, respectively. The polypeptide backbone of the adjacent 2-fold related subunit that contributes Leu 93 to the hydrophobic pocket is colored pink. The silver sphere is the Mg^{2+} ion. The two phenyl groups of benzalate (orange) are accommodated simultaneously within the active site and capped by the amphipathic loop. The locations of the side chains (brown) of Phe 52 and Tyr 54 within the *S*-pocket are also shown.

Scheme 2

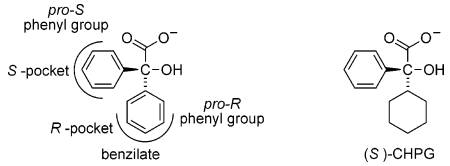

Table 1: Competitive Inhibition of Wild-Type and Mutant Mandelate Racemases

compound	K_i (mM)	
	wild type	F52W/Y54W
benzilate	0.67 ± 0.12	45 ± 4
(*S*)-cyclohexylphenylglycolate	0.50 ± 0.03	nd[a]
diphenylacetate	4.5 ± 0.3	nd[a]
(*R*)-2-hydroxybutyrate	17.3 ± 1.4	98 ± 4
(*S*)-2-hydroxybutyrate	11.4 ± 1.7	71 ± 4

[a] Not determined.

CHPG. Benzilate may be regarded as a substrate-product analogue because it contains the two phenyl groups that would be expected to bind simultaneously in the binding pockets normally occupied by the phenyl group of either (*R*)- or (*S*)-mandelate (Scheme 2). The same is true for (*S*)-CHPG except that one of the phenyl groups is replaced with a cyclohexyl group. Interestingly, wild-type MR bound benzilate and (*S*)-CHPG as competitive inhibitors with affinities that were similar to those exhibited for either substrate enantiomer (Table 1). Although it is possible that benzilate and (*S*)-CHPG may not be bound in the same orientation as the substrate, the observed weak inhibition of MR by diphenylacetate (Table 1) suggests that the presence of two phenyl groups is not sufficient to account for the observed binding affinity of benzilate. In addition, the additional steric bulk within the hydrophobic binding pocket of F52W/Y54W causes a 67-fold reduction in binding affinity for benzilate, relative to that of wild-type MR (Table 1), thereby supporting the notion that benzilate is binding, in part, within the hydrophobic pocket.

Our observations indicate that the active site of MR can accommodate the simultaneous binding of two phenyl rings (or a phenyl ring and a cyclohexyl ring), consistent with the existence of an *R*-pocket and an *S*-pocket for binding the phenyl group within the active site. It is not surprising that MR bound (*S*)-CHPG as well as benzilate since the enzyme binds hexahydromandelate with an affinity similar to that exhibited for mandelate (*19*). Figure 2 shows benzilate modeled into the active site of MR and reveals that the two phenyl groups are accommodated within the active site without significant perturbation of the structure. The *pro-R* phenyl ring of benzilate [equivalent of the phenyl ring of (*R*)-mandelate] occupies a position within the active site where the α-hydrogen of (*S*)-mandelate is observed in X-ray crystal structures (*2*). In the model, the distance between the para carbon atoms of the phenyl rings of bound benzilate is 6.87 Å, similar to the value of 7.128 Å observed in the crystal structure of potassium benzilate (*34*). This distance would certainly accommodate motions of the phenyl ring ranging between 1.8 and 2.8 Å (see Figure 1).

Effect of S-Pocket Mutations on Mandelate Racemization. The ability of MR to simultaneously bind two phenyl rings within its active site suggests that the phenyl ring may move through the hydrophobic cavity of the active site during catalysis. To test this hypothesis, we examined the effect of replacing the side chains of Phe 52 and Tyr 54 with the bulkier side chain of tryptophan. Phe 52 and Tyr 54 comprise part of the hydrophobic *S*-pocket and occupy positions adjacent to the phenyl ring of (*S*)-mandelate (see Figure 5A) but remote from residues involved in polar interactions with ligands, and residues involved in binding the divalent metal ion. Site-directed mutagenesis was used to construct the single mutants F52W and Y54W and the double mutant F52W/Y54W. The added steric bulk in the *S*-pocket was anticipated either to completely block binding of (*S*)-mandelate or to reduce (*S*)-mandelate binding affinity {i.e., increase K_m [$=K_S$ (*16*)] for (*S*)-mandelate}. However, binding of (*R*)-mandelate in the unaltered *R*-pocket of the MR

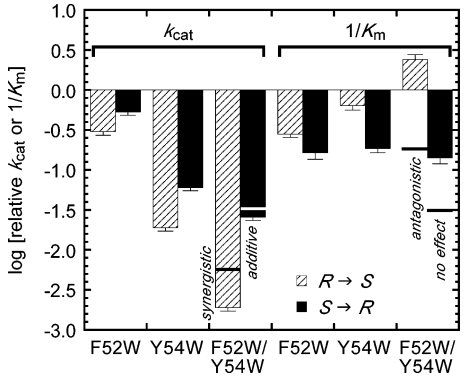

FIGURE 3: Interactions of the effects of the two single mutations (F52W and Y54W) within the *S*-pocket of MR on catalysis (k_{cat}) and substrate binding ($1/K_m$) in the double mutant (F52W/Y54W) with reference to the kinetic parameters of the wild-type enzyme. Values were calculated using the equations $k_{cat}^{rel} = k_{cat}^{mutant}/k_{cat}^{wild-type}$ and $1/K_m^{rel} = K_m^{wild-type}/K_m^{mutant}$. The solid horizontal bars (black or white) on the double mutant columns indicate the product of the effects of the two single mutations, the result expected for additive interactions. Antagonistic, synergistic, and additive effects are indicated.

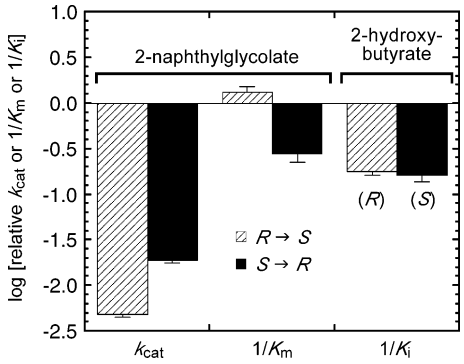

FIGURE 4: Effect of *S*-pocket mutations in F52W/Y54W on 2-naphthylglycolate racemization and 2-hydroxybutyrate binding with reference to the kinetic parameters of the wild-type enzyme. Values were calculated using the equations $k_{cat}^{rel} = k_{cat}^{mutant}/k_{cat}^{wild-type}$, $1/K_m^{rel} = K_m^{wild-type}/K_m^{mutant}$, and $1/K_i^{rel} = K_i^{wild-type}/K_i^{mutant}$.

mutants was not expected to be changed significantly [i.e., no change in K_m for (*R*)-mandelate], and hence, $K_m^{(S)-man} > K_m^{(R)-man}$. From the Haldane relation for a racemase [$K_{eq} = 1 = (k_{cat}/K_m)^{R\rightarrow S}/(k_{cat}/K_m)^{S\rightarrow R}$], one might then expect that $k_{cat}^{R\rightarrow S} < k_{cat}^{S\rightarrow R}$. This rationale is outlined in Scheme 3.[2]

The kinetic parameters for wild-type, F52W, Y54W, and F52W/Y54W MR-catalyzed racemization of mandelate are given in Table 2. As expected, replacement of either Phe 52, Tyr 54, or both Phe 52 and Tyr 54 with tryptophan caused

[2] Similar mutations that increase steric bulk within the putative *R*-pocket would complement our studies. Unfortunately, there are no published X-ray structures of bound (*R*)-mandelate or its analogues, and hence, identification of residues to mutate within the *R*-pocket is not as straightforward as it is for those within the *S*-pocket. Indeed, we have examined residues located where modeling studies suggest that the phenyl ring of (*R*)-mandelate is bound, and it appears that much of the hydrophobic pocket is composed of residues from the β-meander flap that covers the active site. We were reluctant to modify groups on this flap because flap motion and changes in flexibility might confound our interpretation of kinetic results. Other residues within the putative *R*-pocket reside close to the side chain of the general acid−base catalyst Lys 166, and we were concerned that increasing the size of these residues using site-directed mutagenesis would perturb the orientation of Lys 166. Hence, these studies were limited to the putative *S*-pocket.

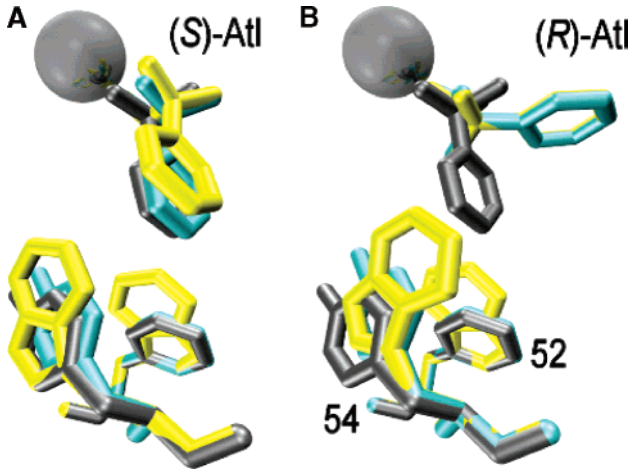

FIGURE 5: MD simulations of the effect of the F52W/Y54W mutations on the binding of (*S*)-atrolactate (A) and (*R*)-atrolactate (B). In both panels, the calculated structure of wild-type MR is shaded blue and the double mutant yellow. For comparison, the residues in wild-type MR with bound (*S*)-atrolactate, as determined by X-ray crystallography [PDB entry 1MDR (*4*)], are colored gray. The Mg^{2+} is shown as a silver sphere.

a 5−7-fold increase in the value of K_m for (*S*)-mandelate relative to that of the wild-type enzyme. On the other hand, the K_m value for (*R*)-mandelate was increased only 3.5-fold for F52W and 1.6-fold for Y54W, and reduced 2.4-fold for the double mutant, relative to that of wild-type MR. For all mutants, enzyme turnover (k_{cat}) was inhibited in both the $S \rightarrow R$ and $R \rightarrow S$ directions. In the $S \rightarrow R$ direction, replacement of Phe 52 with tryptophan caused an only 2-fold reduction in k_{cat}, while replacement of Tyr 54 with tryptophan caused a 17-fold reduction in k_{cat}. The greatest reduction in k_{cat} (~40-fold) in the $S \rightarrow R$ direction was observed with the double mutant. In the $R \rightarrow S$ direction, replacement of Phe 52 with tryptophan caused an only 3-fold reduction in k_{cat}, while replacement of Tyr 54 with tryptophan caused a 53-fold reduction in k_{cat}. For the double mutant, there was a marked reduction in k_{cat} (~526-fold) in the $R \rightarrow S$ direction. Although catalysis is impaired in both the $S \rightarrow R$ and $R \rightarrow S$ directions for all the mutants that were generated, it is important to note that in all cases the $k_{cat}^{R\rightarrow S}/k_{cat}^{S\rightarrow R}$ ratio decreases from a value of 1.13 for wild-type MR to values of 0.64, 0.36, and 0.08 for F52W, Y54W, and F52W/Y54W, respectively.

Mildvan and co-workers (*35*, *36*) have pointed out that the quantitative effect of a second mutation on a mutant enzyme may be antagonistic (or suppressive), absent, partially additive, or synergistic with respect to the first mutation. Figure 3 illustrates the interactions of the effects of the two single mutations on catalysis (k_{cat}) and substrate binding ($1/K_m$) in the double mutant relative to wild-type MR. The introduction of a second tryptophan residue has either a synergistic ($R \rightarrow S$) or additive ($S \rightarrow R$) effect on the reduction of k_{cat}. On the other hand, the second mutation has little effect on the binding of (*S*)-mandelate and an antagonistic effect on the inhibition of (*R*)-mandelate binding such that the binding of (*R*)-mandelate is actually enhanced in the double mutant. These observations suggest that once the steric bulk is increased in the *S*-pocket by introduction of the tryptophan residue, additional steric bulk due to a second tryptophan residue does not further inhibit binding of (*S*)-mandelate. However, the effects the F52W and Y54W

Scheme 3

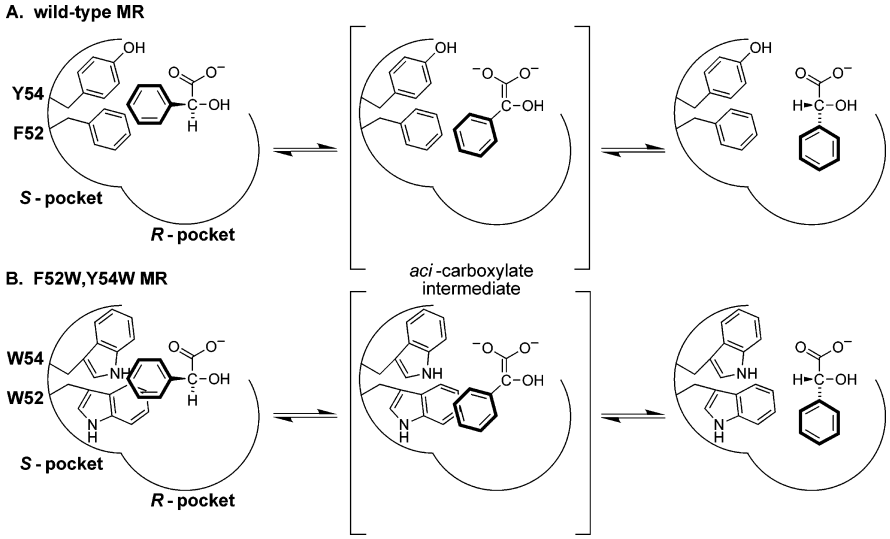

Table 2: Kinetic Parameters for Wild-Type and Mutant Mandelate Racemases Acting on Mandelate

	wild type	F52W	Y54W	F52W/Y54W
% α content	32.5 (40.4)[a]	31.0	31.2	32.1
% β content	19.1 (19.5)[a]	20.4	19.9	18.7
$K_A(Mg^{2+})$ (mM)	0.21 ± 0.06	0.07 ± 0.02	2.3 ± 0.2	0.15 ± 0.02
K_i(benzohydroxamate) (μM)	12 ± 1	63 ± 10	110 ± 10[b]	640 ± 190
K_{eq} [$=(k_{cat}/K_m)^{R\rightarrow S}/(k_{cat}/K_m)^{S\rightarrow R}$]	1.1 ± 0.1	0.8 ± 0.1	0.9 ± 0.1	1.1 ± 0.1
		$R \rightarrow S$		
k_{cat} (s^{-1})	526 ± 17	159 ± 17	10 ± 1[b]	1.0 ± 0.1
K_m (mM)	0.70 ± 0.06	2.5 ± 0.1	1.1 ± 0.1[b]	0.29 ± 0.03
k_{cat}/K_m (M^{-1} s^{-1})	(7.7 ± 0.8) × 10^5	(6.4 ± 0.5) × 10^4	(9.3 ± 0.4) × 10^3 [b]	(3.5 ± 0.1) × 10^3
		$S \rightarrow R$		
k_{cat} (s^{-1})	467 ± 24	248 ± 20	28 ± 2[b]	12 ± 1
K_m (mM)	0.54 ± 0.06	3.3 ± 0.5	2.9 ± 0.2[b]	3.8 ± 0.5
k_{cat}/K_m (M^{-1} s^{-1})	(8.7 ± 0.5) × 10^5	(7.7 ± 0.9) × 10^4	(9.9 ± 1.3) × 10^3 [b]	(3.1 ± 0.4) × 10^3

[a] The secondary structure content reported for the X-ray crystal structure of wild-type MR bound with (*S*)-atrolactate (*4*) is shown in parentheses. [b] Value determined using a Mg^{2+} concentration of 15 mM.

mutations are not limited solely to the *S*-pocket but appear to be global as indicated by the overall reduction in the level of catalysis for all mutant enzymes (vide infra).

MR has been regarded as a pseudosymmetric enzyme because it catalyzes the racemization of either (*R*)- or (*S*)-mandelate with nearly identical kinetic constants (*37*). However, in fact, a subtle "asymmetry" in the kinetic parameters does exist. As shown in Table 2, wild-type MR exhibits a slightly higher affinity for (*S*)-mandelate [i.e., $K_m^{(S)-man} < K_m^{(R)-man}$] but catalyzes the turnover of (*R*)-mandelate slightly more rapidly (i.e., $k_{cat}^{R\rightarrow S} > k_{cat}^{S\rightarrow R}$) (*16*). All of the MR variants in this study exhibit greater turnover numbers for (*S*)-mandelate than for (*R*)-mandelate, yet have higher affinity for (*R*)-mandelate than for (*S*)-mandelate. This reversal of catalytic preference is in accord with our expectation that movement of the phenyl ring of (*R*)-mandelate into the obstructed *S*-pocket is unfavorable (Scheme 3). Similar, but less pronounced, reversals of catalytic preference have also been reported for the K166R (*3*) and D270N (*6*) mutants of MR.

For all mutants examined in this study, the efficiency (k_{cat}/K_m) was reduced. In both the $S \rightarrow R$ and $R \rightarrow S$ directions, the efficiency was reduced only 12-fold upon replacement of Phe 52 with tryptophan, while replacement of Tyr 54 with tryptophan caused a much more significant ~85-fold reduction in efficiency. The double mutant exhibited the greatest reduction in efficiency (~250-fold), relative to that of wild-type MR. The reduction in the catalytic efficiency of the mutants is paralleled by the reduction in the binding affinity of the intermediate/transition-state analogue benzohydroxamate (Table 2). In all cases, the values of k_{cat}/K_m in the $S \rightarrow R$ and $R \rightarrow S$ directions were experimentally equal, giving values of unity for the equilibrium constants as expected from the Haldane relationship (*38*) (Table 2).

It is not surprising that the introduction of steric bulk into the *S*-pocket causes a reduction in the catalytic efficiency since addition of new functional groups to amino acid side chains may cause local reorganization of structure (*39*). Although circular dichroism measurements indicated that the mutations did not introduce any gross changes in the overall secondary structure of the protein (Table 2), it is possible that the added bulk may have subtly perturbed the spatial arrangement of active site residues. An indication of such a perturbation is the altered affinity that the mutants exhibited for Mg^{2+}. Replacement of Phe 52 with tryptophan caused a slight increase in the apparent affinity for Mg^{2+} (~3-fold, Table 2), while replacement of Tyr 54 with tryptophan had the opposite effect, decreasing the apparent affinity for Mg^{2+} by 11-fold. For this reason, kinetic studies with the Y54W mutant were conducted with the Mg^{2+} concentration equal

Table 3: Kinetic Parameters for Wild-Type and Mutant Mandelate Racemases Acting on the Enantiomers of 2-Naphthylglycolate

	wild type[a]	F52W/Y54W
	$R \rightarrow S$	
k_{cat} (s^{-1})	33 ± 1	0.16 ± 0.01
K_m (mM)	0.46 ± 0.06	0.35 ± 0.03
k_{cat}/K_m (M^{-1} s^{-1})	$(7.17 \pm 0.96) \times 10^4$	$(4.57 \pm 0.48) \times 10^2$
	$S \rightarrow R$	
k_{cat} (s^{-1})	25 ± 1	0.48 ± 0.03
K_m (mM)	0.41 ± 0.03	1.5 ± 0.3
k_{cat}/K_m (M^{-1} s^{-1})	$(6.1 \pm 0.5) \times 10^4$	$(3.20 \pm 0.67) \times 10^2$

[a] Values from ref *19*.

to 15 mM to ensure saturation of the mutant enzyme. Interestingly, the two opposite effects on the apparent affinity for Mg^{2+} observed for the F52W and Y54W mutants seemed to cancel each other out in the double mutant.

Effect of S-Pocket Mutations on 2-Naphthylglycolate Racemization and 2-Hydroxybutyrate Binding. 2-Naphthylglycolate is a bulky substrate (*19*) and is expected to be more sensitive to additional steric bulk in the *S*-pocket. The kinetic parameters for wild-type and F52W/Y54W MR-catalyzed racemization of 2-naphthylglycolate are given in Table 3, and the effects of the double mutation on catalysis (k_{cat}) and substrate binding ($1/K_m$) in the $S \rightarrow R$ and $R \rightarrow S$ directions, relative to those of wild-type MR, are shown in Figure 4. While wild-type MR exhibits approximately equal affinity for both (*R*)- and (*S*)-2-naphthylglycolate, F52W/Y54W exhibits an approximately 4-fold higher affinity for (*R*)-2-naphthylglycolate than for the (*S*)-enantiomer. This is less than the corresponding 13-fold binding preference exhibited by F52W/Y54W for (*R*)-mandelate over (*S*)-mandelate. The value of $k_{cat}^{R\rightarrow S}/k_{cat}^{S\rightarrow R}$ decreases from a value of 1.32 for wild-type MR to 0.33 for F52W/Y54W. Although the changes in k_{cat} and K_m for 2-naphthylglycolate racemization follow the same trend observed for mandelate racemization, 2-naphthylglycolate is not *more* sensitive to the bulkier steric bulk in the *S*-pocket. This apparent lack of sensitivity, relative to mandelate, may arise because the bulkier 2-naphthylglycolate is more sensitive to structural perturbations that alter k_{cat} in the double mutant. We have shown previously that steric constraints within the hydrophobic cavity of the enzyme−intermediate complex are more stringent than those in the enzyme−substrate complex, leading to weakened transition-state/intermediate stabilization during 2-naphthylglycolate racemization (*19*).

On the other hand, the substrate analogues (*R*)- and (*S*)-2-hydroxybutyrate are expected to be less sensitive to the additional steric bulk in the *S*-pocket. Although these substrate analogues are weak competitive inhibitors of wild-type and F52W/Y54W MRs (Table 1), both the wild-type and double mutant enzymes exhibit higher affinity for (*S*)-2-hydroxybutyrate than for (*R*)-2-hydroxybutyrate, in accord with our expectation (Figure 4). Interestingly, the affinity for both (*R*)- and (*S*)-2-hydroxybutyrate was markedly reduced in the double mutant. Again, this is consistent with the presence of more global structural perturbations within the active site of F52W/Y54W.

Molecular Dynamics Simulations. To obtain a better understanding of how increased steric bulk within the *S*-pocket perturbs substrate binding, the binding of (*S*)-atrolactate and (*R*)-atrolactate to wild-type MR and F52W/Y54W was modeled (Figure 5). Atrolactate was chosen as the ligand for the modeling studies because the accuracy of the modeling could be assessed by direct comparison with the crystal structure of wild-type MR with bound (*S*)-atrolactate [PDB entry 1MDR (*4*)]. In our MD simulations, atrolactate was observed to move slightly away from the coordination sphere of the Mg^{2+} ion. Attempts to distribute the partial charges on the inhibitor using various approaches (AM1, PM3, MINDO/3, and MNDO) with Mopac 6.0 (*40*) did not reduce the drift. Indeed, the drift appears to be due to the absence of an octahedral geometry for the coordination of Mg^{2+} in the model and the stronger electrostatic interaction of the carboxylate group of atrolactate with the divalent magnesium ion than with Glu 317. However, the models presented in Figure 5 do simulate the proper coordination of Mg^{2+} by atrolactate by setting a distance constraint between these two species.

As shown in Figure 5, the MD simulations reveal that the presence of the two tryptophan side chains in F52W/Y54W causes the phenyl ring of (*S*)-atrolactate to assume a different orientation within the active site relative to that assumed in the wild-type·(*S*)-atrolactate complex. On the other hand, the orientation of the phenyl ring of (*R*)-atrolactate is not significantly altered relative to its orientation in the wild-type·(*R*)-atrolactate complex. These observations are consistent with our kinetic results.

Conclusions. Despite the overall reduction in catalytic efficiency of the mutant enzymes, it is clear that replacement of either Phe 52, Tyr 54, or both residues with tryptophan causes a reduction in $k_{cat}^{R\rightarrow S}$ relative to $k_{cat}^{S\rightarrow R}$, and an increase in $K_m^{(S)-man}$ relative to $K_m^{(R)-man}$ for mandelate racemization, with the changes being most striking in the double mutant. Thus, increased steric bulk within the *S*-pocket introduces "asymmetry" into the kinetics of mandelate racemase catalysis by decreasing the binding affinity for (*S*)-mandelate and decreasing the turnover number for formation of (*S*)-mandelate. Such a reversal of enantioselective binding affinity is not observed for the substrate analogues (*S*)- and (*R*)-2-hydroxybutyrate which are expected to be less sensitive to additional steric bulk in the *S*-pocket. These findings are consistent with the notion that the phenyl group of the substrate moves through the active site during catalysis. Although the magnitude of this motion remains unknown, such motion through the "greasy" hydrophobic pocket of the active site should be facile since only weak (∼2−4 kcal/mol) hydrophobic interactions are involved in binding the phenyl ring in the ground state (*19*). Recognition that specific functional groups attached to the stereocenter of a substrate undergoing racemization may move during catalysis has important implications for the design of inhibitors for racemases and epimerases. Geminal substitution on the stereocenter of the substrate with the functional group undergoing motion may be a useful strategy for generating competitive inhibitors (e.g., the *gem*-phenyl groups on benzilate).

ACKNOWLEDGMENT

We thank Dr. Alex R. Jurgens (Sepracor Canada Ltd.) for kindly providing us with a sample of (*S*)-CHPG.

REFERENCES

1. Gerlt, J. A. (1998) Enzyme-Catalyzed Proton Transfer Reactions to and from Carbon, in *Bioorganic Chemistry: Peptides and*

Proteins (Hecht, S. M., Ed.) pp 279−311, Oxford University Press, New York.
2. Neidhart, D. J., Howell, P. L., Petsko, G. A., Powers, V. M., Li, R. S., Kenyon, G. L., and Gerlt, J. A. (1991) Mechanism of the reaction catalyzed by mandelate racemase. 2. Crystal structure of mandelate racemase at 2.5-Å resolution: Identification of the active site and possible catalytic residues, *Biochemistry 30*, 9264−9273.
3. Kallarakal, A. T., Mitra, B., Kozarich, J. W., Gerlt, J. A., Clifton, J. G., Petsko, G. A., and Kenyon, G. L. (1995) Mechanism of the reaction catalyzed by mandelate racemase: Structure and mechanistic properties of the K166R mutant, *Biochemistry 34*, 2788−2797.
4. Landro, J. A., Gerlt, J. A., Kozarich, J. W., Koo, C. W., Shah, V. J., Kenyon, G. L., Neidhart, D. J., Fujita, S., and Petsko, G. A. (1994) The role of lysine 166 in the mechanism of mandelate racemase from *Pseudomonas putida*: Mechanistic and crystallographic evidence for stereospecific alkylation by (*R*)-α-phenylglycidate, *Biochemistry 33*, 635−643.
5. Mitra, B., Kallarakal, A. T., Kozarich, J. W., Gerlt, J. A., Clifton, J. G., Petsko, G. A., and Kenyon, G. L. (1995) Mechanism of the reaction catalyzed by mandelate racemase: Importance of electrophilic catalysis by glutamic acid 317, *Biochemistry 34*, 2777−2787.
6. Schafer, S. L., Barrett, W. C., Kallarakal, A. T., Mitra, B., Kozarich, J. W., Gerlt, J. A., Clifton, J. G., Petsko, G. A., and Kenyon, G. L. (1996) Mechanism of the reaction catalyzed by mandelate racemase: Structure and mechanistic properties of the D270N mutant, *Biochemistry 35*, 5662−5669.
7. Powers, V. M., Koo, C. W., Kenyon, G. L., Gerlt, J. A., and Kozarich, J. W. (1991) Mechanism of the reaction catalyzed by mandelate racemase. 1. Chemical and kinetic evidence for a two-base mechanism, *Biochemistry 30*, 9255−9263.
8. St. Maurice, M., and Bearne, S. L. (2000) Reaction intermediate analogues for mandelate racemase: Interaction between Asn 197 and the α-hydroxyl of the substrate promotes catalysis, *Biochemistry 39*, 13324−13335.
9. Chiang, Y., Kresge, A. J., Pruszynski, P., Schepp, N. P., and Wirz, J. (1990) The enol of mandelic acid, detection, acidity in aqueous solution, and estimation of the keto−enol equilibrium constant and carbon acidity of mandelic acid, *Angew. Chem., Int. Ed. Engl. 29*, 792−794.
10. Gerlt, J. A., and Gassman, P. G. (1993) Understanding the rates of certain enzyme-catalyzed reactions: Proton abstraction from carbon acids, acyl-transfer reactions, and displacement reactions of phosphodiesters, *Biochemistry 32*, 11943−11952.
11. Gerlt, J. A., and Gassman, P. G. (1993) An explanation for rapid enzyme-catalyzed proton abstraction from carbon acids: Importance of late transition states in concerted mechanisms, *J. Am. Chem. Soc. 115*, 11552−11568.
12. Babbitt, P. C., and Gerlt, J. A. (1997) Understanding enzyme superfamilies. Chemistry as the fundamental determinant in the evolution of new catalytic activities, *J. Biol. Chem. 272*, 30591−30594.
13. Babbitt, P. C., Hasson, M. S., Wedekind, J. E., Palmer, D. R., Barrett, W. C., Reed, G. H., Rayment, I., Ringe, D., Kenyon, G. L., and Gerlt, J. A. (1996) The enolase superfamily: A general strategy for enzyme-catalyzed abstraction of the α-protons of carboxylic acids, *Biochemistry 35*, 16489−16501.
14. Gerlt, J. A., Kenyon, G. L., Kozarich, J. W., Neidhart, D. C., and Petsko, G. A. (1992) Mandelate racemase and class-related enzymes, *Curr. Opin. Struct. Biol. 2*, 736−742.
15. Bearne, S. L., and Wolfenden, R. (1997) Mandelate racemase in pieces: Effective concentrations of enzyme functional groups in the transition state, *Biochemistry 36*, 1646−1656.
16. St. Maurice, M., and Bearne, S. L. (2002) Kinetics and thermodynamics of mandelate racemase catalysis, *Biochemistry 41*, 4048−4058.
17. Wolfenden, R., Snider, M. J., Ridgway, C., and Miller, B. (1999) The temperature dependence of enzyme rate enhancements, *J. Am. Chem. Soc. 121*, 7419−7420.
18. Felfer, U., Strauss, U. T., Kroutil, W., Fabian, W. M. F., and Faber, K. (2001) Substrate spectrum of mandelate racemase: Part 2. (Hetero)-aryl-substituted mandelate derivatives and modulation of activity, *J. Mol. Catal. B: Enzym. 15*, 213−222.
19. St. Maurice, M., and Bearne, S. L. (2004) Hydrophobic Nature of the Active Site of Mandelate Racemase, *Biochemistry 43*, 2524−2532.
20. Bearne, S. L., St. Maurice, M., and Vaughan, M. D. (1999) An assay for mandelate racemase using high-performance liquid chromatography, *Anal. Biochem. 269*, 332−336.
21. Sharp, T. R., Hegeman, G. D., and Kenyon, G. L. (1979) A direct kinetic assay for mandelate racemase using circular dichroic measurements, *Anal. Biochem. 94*, 329−334.
22. Fee, J. A., Hegeman, G. D., and Kenyon, G. L. (1974) Mandelate racemase from *Pseudomonas putida*. Subunit composition and absolute divalent metal ion requirement, *Biochemistry 13*, 2528−2532.
23. Böhm, G., Muhr, R., and Jaenicke, R. (1992) Quantitative analysis of protein far UV circular dichroism spectra by neural networks, *Protein Eng. 5*, 191−195.
24. Brooks, B. R., Bruccoleri, R. E., Olafson, B. D., States, D. J., Swaminathan, S., and Karplus, M. (1983) CHARMM: A program form macromolecular energy, minimization, and dynamics calculations, *J. Comput. Chem. 4*, 187−217.
25. MacKerell, A. D. J., Bashford, D., Bellott, M., Dunbrack, R. L. J., Evanseck, J. D., Field, M. J., Fischer, S., Gao, J., Guo, H., Joseph-McCarthy, D., Kuchnir, L., Kuczera, K., Lau, F. T. K., Mattos, C., Michnick, S., Ngo, T., Nguyen, D. T., Prodhom, B., Reiher, W. E., Roux, B., Schlenkrich, M., Smith, J. C., Stote, R., Straub, J., Watanabe, M., Wiórkiewicz-Kuczera, J., Yin, D., and Karplus, M. (1998) All-Atom Empirical Potential for Molecular Modeling and Dynamics Studies of Proteins, *J. Phys. Chem. B 102*, 3586−3616.
26. Schuttelkopf, A. W., and van Aalten, D. M. (2004) PRODRG: A tool for high-throughput crystallography of protein−ligand complexes, *Acta Crystallogr. D60*, 1355−1363.
27. Dominy, D., and Brooks, C. L. I. (1999) Development of a Generalized Born Model Parameterization for Proteins and Nucleic Acids, *J. Phys. Chem. B 103*, 3765−3773.
28. Garcia-Viloca, M., Gonzalez-Lafont, A., and Lluch, J. M. (2001) A QM/MM study of the racemization of vinylglycolate catalyzed by mandelate racemase enzyme, *J. Am. Chem. Soc. 123*, 709−721.
29. Van Gunsteren, W. F., and Berendsen, H. J. C. (1977) Algorithms for macromolecular dynamics and constraint dynamics, *Mol. Phys. 34*, 1311−1327.
30. Kenyon, G. L., and Hegeman, G. D. (1970) Mandelic acid racemase from *Pseudomonas putida*. Evidence favoring a carbanion intermediate in the mechanism of action, *Biochemistry 9*, 4036−4043.
31. Lin, D. T., Powers, V. M., Reynolds, L. J., Whitman, C. P., Kozarich, J. W., and Kenyon, G. L. (1988) Evidence for the generation of α-carboxy-α-hydroxy-*p*-xylylene from *p*-(bromomethyl)mandelate by mandelate racemase, *J. Am. Chem. Soc. 110*, 323−324.
32. Landro, J. A., Kenyon, G. L., and Kozarich, J. W. (1992) Mechanism-based inactivation of mandelate racemase by propargylglycolate, *Bioorg. Med. Chem. Lett. 2*, 1411−1418.
33. Li, R., Powers, V. M., Kozarich, J. W., and Kenyon, G. L. (1995) Racemization of vinylglycolate catalyzed by mandelate racemase, *J. Org. Chem. 60*, 3347−3351.
34. Rojas, L. S., Ramírez, B. M., Mora, A. J., Delgado, G. E., and de Delgado, G. D. (2003) Redetermination of potassium benzilate, *Acta Crystallogr. E59*, m647−m651.
35. Mildvan, A. S. (2004) Inverse Thinking about Double Mutants of Enzymes, *Biochemistry 43*, 14517−14520.
36. Mildvan, A. S., Weber, D. J., and Kuliopulos, A. (1992) Quantitative Interpretations of Double Mutations of Enzymes, *Arch. Biochem. Biophys. 294*, 327−340.
37. Whitman, C. P., Hegeman, G. D., Cleland, W. W., and Kenyon, G. L. (1985) Symmetry and asymmetry in mandelate racemase catalysis, *Biochemistry 24*, 3936−3942.
38. Segel, I. H. (1975) *Enzyme Kinetics*, John Wiley and Sons, Inc., New York.
39. Fersht, A. (1999) *Structure and Mechanism in Protein Science*, W. H. Freeman and Co., New York.
40. Stewart, J. J. (1990) MOPAC: A semiempirical molecular orbital program, *J. Comput.-Aided Mol. Des. 4*, 1−105.
41. Mesecar, A. D., and Koshland, D. E., Jr. (2000) A new model for protein stereospecificity, *Nature 403*, 614−615.

BI0473096